Fatigue Crack Growth Behavior of a New Single Crystal Nickel-Based Superalloy (CMSX-4) at 650 °C

A. Sengupta, S.K. Putatunda, and M. Balogh

The fatigue crack growth behavior of a new single crystal nickel-based superalloy containing rhenium (CMSX-4) has been studied at 650 °C. The investigation also examined the influence of γ′ precipitates (size and distribution) on the near-threshold fatigue crack growth rate and the fatigue threshold. The influence of load ratio on the fatigue crack growth rate and the fatigue threshold was also examined. Detailed fractographic studies were carried out to determine the crack growth mechanism in fatigue in the threshold region. Compact tension specimens were prepared from the single crystal nickel-based superalloy CMSX-4 with [001] orientation as the tensile loading axis direction. These specimens were given three different heat treatments to produce three different γ′ precipitate sizes and distributions. Fatigue crack growth behavior of these specimens was studied at 650 °C in air.

The results of the present investigation indicate that the near-threshold fatigue crack growth rate decreases and that the fatigue threshold increases with an increase in the γ′ precipitate size at 650 °C. The fatigue threshold decreased linearly with an increase in load ratio. Fractographs at 650 °C show a stage II type of crack growth along {100} type of crystal planes in the threshold region, and along {111} type of crystal planes in the high ΔK region.

Keywords

fatigue crack growth, high temperature, nickel superalloy, single crystal

1. Introduction

FATIGUE crack growth rate has been related to the stress intensity range, (ΔK) and the Paris equation (Ref 1) has been found to be very useful in characterizing the fatigue crack growth behavior of structural components. The useful life of a structural component subjected to cyclic loading or fatigue can be determined by the time required for cracks or flaws already present in a structural component to grow from a subcritical dimension to a critical size. The critical flaw size under a given loading condition is determined by the plain strain fracture toughness, K_{IC} (Ref 2) of the material. The Paris equation relates the crack growth rate, da/dN, to the stress-intensity range, ΔK, in the form of a power law:

$$da/dN = C(\Delta K)^m$$

where C and m are material constants and $\Delta K = K_{max} - K_{min}$ is the difference between maximum and minimum stress intensity factors.

However, when experimental crack growth rate data is plotted against the stress-intensity range in a log-log scale, a sigmoidal curve with varying slopes is obtained, as opposed to a linear plot as predicted by the Paris equation. There are three distinct regions in this plot. In region I, or the threshold region, the crack growth rate is very slow and deviates from the Paris equation. In region II, or the linear region, the Paris equation is usually obeyed by most materials, and the crack growth rate increases linearly with the stress-intensity factor. In region III, or the fast fracture region, the crack growth rate accelerates and again deviates from the Paris equation. In addition to these three regions, there is also a threshold stress-intensity factor (ΔK_{th}), below which the crack growth rate approaches a zero value.

The threshold region is very important, because a significant portion of the life of a structural component is spent in this region. The threshold stress-intensity factor is also a very important parameter for structural design, because components designed on the basis of the fatigue threshold are expected to have infinite lives. The near-threshold crack growth rate and the fatigue threshold are known to be microstructurally sensitive. Therefore, microstructural modifications appear to be the only possible way to improve the near-threshold fatigue crack growth resistance and the fatigue threshold. In nickel-based superalloys, (Ref 3-6) these properties are expected to be dependent on the γ′ precipitate size and distribution. However, very little information is available in the literature regarding the influence of γ′ precipitate size on the near-threshold fatigue crack growth rate and the fatigue threshold at elevated temperatures, in the case of single crystal nickel-based superalloys.

CMSX-4 is a recently developed (Ref 7, 8) rhenium containing single crystal nickel-based superalloy. This alloy has potential applications in many critical high-temperature applications such as turbine blades, rotors, nuclear reactors, etc. The fatigue crack growth rate and the fatigue threshold data of this material is extremely important for accurate life prediction, as well as failure safe design, at elevated temperatures.

The present investigation was undertaken to determine the influence of γ′ precipitates on the fatigue crack growth rate and the fatigue threshold of the single crystal nickel-based superalloy CMSX-4 at a temperature of 650 °C. Detailed fractographic studies were carried out to determine the crack growth mechanism in fatigue at both the threshold and high ΔK region in this

A. Sengupta and **S.K. Putatunda,** Department of Materials Science and Engineering, Wayne State University, Detroit, MI, USA; and **M. Balogh,** General Motors Technical Center, Warren, MI, USA

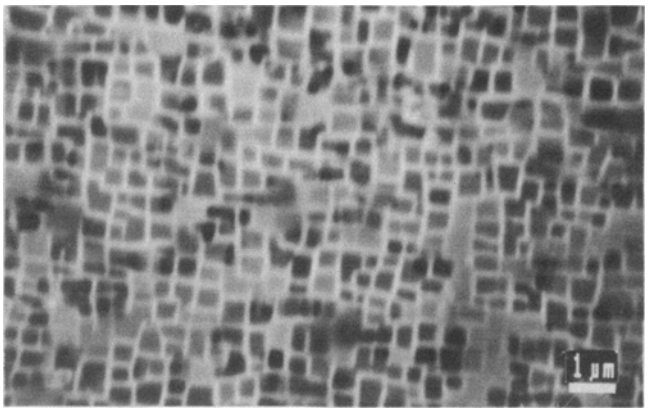

(a)

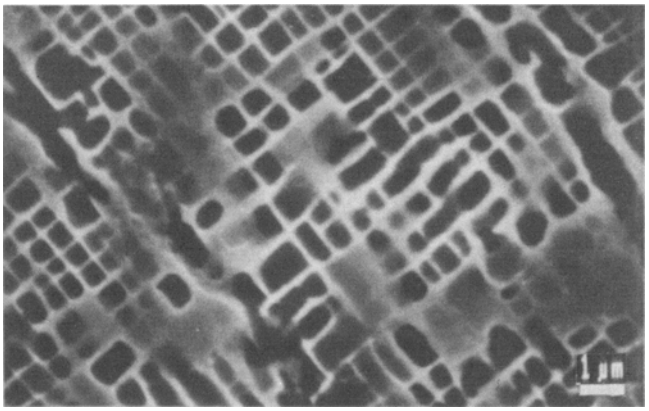

(b)

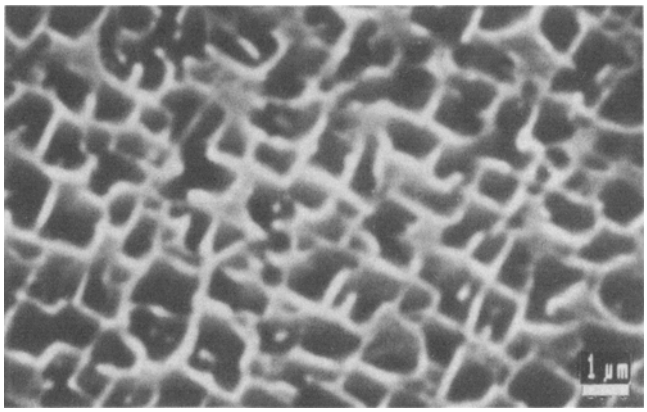

(c)

Fig. 1 (a) Microstructure of the material in heat treated condition A. (b) Microstructure of the material in heat treated condition B. (c) Microstructure of the material in heat treated condition C

alloy. The influence of load ratio or mean stress on the fatigue crack growth rate and the fatigue threshold was also examined.

2. Experimental Procedures

2.1 *Material*

The material used in this investigation was the single crystal nickel-based superalloy CMSX-4. The chemical composition of the material (in wt%) is 6.5 Cr, 10.0 Co, 0.6 Mo, 6.5 W, 6.5 Ta, 3.0 Re, 5.5 Al, 1.0 Ti, 0.1 Hf, and the balance nickel. The master alloy was vacuum cast and single crystals were grown by a modified Bridgemann technique (Ref 9). The crystals were grown in [001] orientation. The orientation of these crystals was verified by the back reflection Laue method.

2.2 *Specimen Preparation*

The cast alloy was available in the form of a 62.5 mm × 62.5 mm × 12.5 mm block. For fatigue testing, 2 (T) compact tension specimens were prepared following ASTM Standard E-647 (Ref 10). The specimens were fabricated using an electrical discharge machine (EDM). The loading axis of these specimens was kept in [001] direction. The width of the specimens was kept at 50.8 mm (2 in.) and the thickness to 6.25 mm (0.25 in.). The aspect ratio was kept at a/W = 0.30. Standard back reflection X-ray diffraction (Laue) was performed on all these specimens after machining to verify their orientations. The crack growth direction was in [100] direction.

2.3 *Heat Treatments*

After fabrication, the specimens were subjected to three different heat treatments. These heat treated conditions are termed as heat treated contition A, B, and C respectively. The details of these heat treatments are listed below.

- *Heat treated condition A:* As-received bars were solution treated at 1276 °C for 2 hours; at 1287 °C for 2 hours; at 1296 °C for 3 hours; at 1304 °C for 3 hours; at 1315 °C for 2 hours; at 1315 °C for 2 hours; at 1321 °C for 2 hours; at 1324 °C for 2 hours; then finally air cooled. Following this solution treatment the bars were subjected to high temperature aging at 1080 °C for 4 hours, then air cooled. Final aging at 871 °C for 20 hours, then finally air cooled. Resultant average γ' size is 0.3 μm.
- *Heat treated condition B:* Two step aging (after heat treatment condition A). Aged at 1140 °C for 6 hours, then air

Table 1 Mechanical properties of the material

Material condition	Temperature, °C	Yield strength, MPa	Ultimate tensile strength, MPa	Young's modulus, GPa	Elongation, %
A	24	888	894	133	22.0
B	24	942	942	133	17.5
C	24	934	934	133	24.3
A	650	920	1016	100	11.4
B	650	947	1064	100	11.8
C	650	1024	1128	100	7.5

cooled; final aging at 871 °C for 100 hours, then finally air cooled. Resultant average γ' size is 0.5 μm.

- *Heat treated condition C:* After heat treatment A, 1290 °C for 4 hours, then air cooled, solution treated at 1290 °C for 2 hours, followed by water quench, then high temperature aging at 1080 °C for 4 hours, then air cooled; final aging at 871 °C for 1000 hours, then finally air cooled. Resultant average γ' size is 0.9 μm.

The resultant microstructures are shown in Fig. 1(a), (b), and (c). Heat treatment A resulted in an average γ' precipitate size of 0.3 μm. Heat treatments B and C produced average γ' sizes of 0.5 μm and 0.9 μm, respectively. The volume fraction and size of γ' precipitates were determined using an, image analyzer (Ref 11-13). The γ' precipitates produced by the heat treatments were cuboidal in nature. The volume fraction of γ' precipitates was in the range of 65 to 70 percent (Ref 11-13) in all these specimens. The mechanical properties of these materials at room temperature and at 650 °C were determined by tensile testing of three to four identical test samples (also of [001] orientation) in each heat treated condition at room temperature and 650 °C. The average values from these specimens are reported in Table 1.

2.4 *Fatigue Testing*

After heat treatment, the compact tension specimens were polished on both surfaces with 600 grit emery paper. Then they were cleaned and degreased in acetone. This procedure was very helpful in locating the crack tip during the fatigue testing.

The specimens were initially precracked in fatigue at a ΔK level of 20 MPa · $m^{1/2}$ to produce a 2 mm long sharp crack front in accordance with ASTM Standard E-647 (Ref 10). After fatigue precracking, fatigue testing was carried out in a servohydraulic MTS test machine using the load control mode. The crack lengths and number of cycles for crack growth were recorded continuously. A constant amplitude sinusoidal wave form was applied and the tests were carried out at various load ratios, such as R = 0.1, 0.3 and 0.5. All tests were carried out at a constant cyclic frequency of ten cycles per second in the threshold region in ambient atmosphere at 650 °C.

The specimens were enclosed in a high-temperature environmental chamber. The temperature of the chamber was controlled within ± 2 °C with the help of a temperature controller. This chamber was equipped with a transparent quartz window. Crack lengths on the surface of the test specimens were monitored through this window with the help of an optical traveling microscope. A photograph of the experimental setup is shown in Fig. 2. All tests were carried out in air at 650 °C.

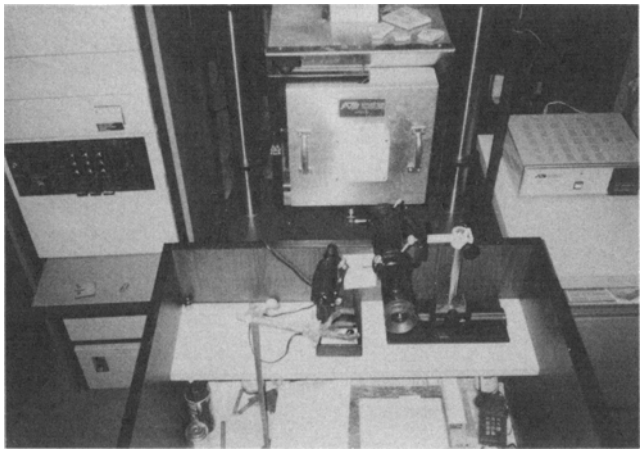

Fig. 2 Environmental chamber used for high temperature fatigue studies

The fatigue threshold was determined using the load shedding technique as specified in ASTM Standard E-647 (Ref 10). For this purpose, the load values were gradually decreased and the crack growth rates were continuously recorded. This load reduction at any ΔK level was done only up to a maximum of 5%, and also only after the crack had grown by at least 2 mm at the previous ΔK level. In this way, any retardation effect due to the prior ΔK was avoided.

The crack growth rate (da/dN) and ΔK were determined using the incremental polynomial method of ASTM Standard E-647 (Ref 10). These were then plotted in terms of log da/dN versus log ΔK. The threshold was identified graphically from these plots following ASTM Standard E-647 (Ref 10). The threshold was identified as the ΔK level at which crack growth rate was of the order of 10^{-10} m/cycle as per ASTM Standard E-647 (Ref 10). Three to four identical test specimens were tested from each heat treated condition A, B, and C at each load ratio (R = 0.1, 0.3 and 0.5) at 650 °C. The average values from these specimens were then taken as the representative of the crack growth rate data and the fatigue threshold.

3. Results and Discussion

3.1 *Influence of γ' Precipitate Size on the Fatigue Crack Growth Rate and the Fatigue Threshold*

Tensile test results reported in Table 1 show that both yield and tensile strength of the material increase with an increase in

γ' precipitate size. Furthermore, the test results show that there is a significant decrease in ductility and an increase in ultimate tensile strength at 650 °C compared to room temperature. This behavior is indicative of dynamic strain aging (Ref 12) in this material at 650 °C.

Figure 3 compares the fatigue crack growth behavior of CMSX-4 for heat treated conditions A, B, and C at 650 °C at the same load ratio of R = 0.1. Similarly, Fig. 4 and 5 compare the fatigue crack growth behavior of the material at heat treated conditions A, B, and C at load ratios of R = 0.3 and R = 0.5, respectively. In Table 2, the fatigue threshold data of these materials are reported at 650 °C.

It is evident from Fig. 3, 4, and 5 that the fatigue crack growth rate of heat treated condition A material is higher than heat treated conditions B and C materials. In the threshold region, the difference in the crack growth rates is significant.

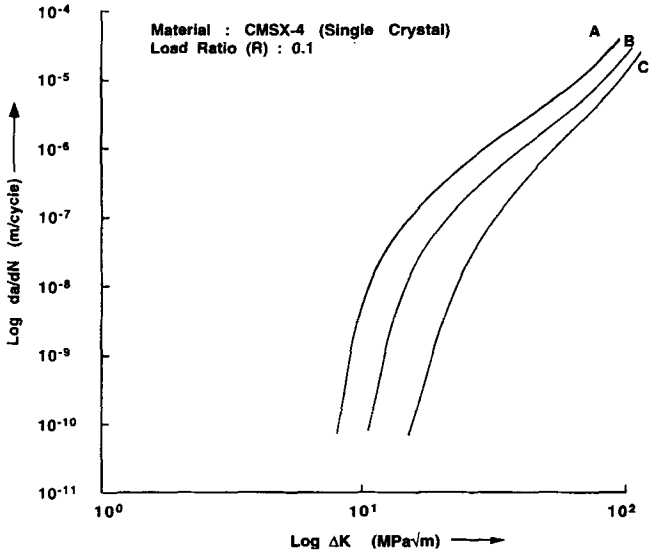

Fig. 3 Fatigue crack growth behavior at 650 °C

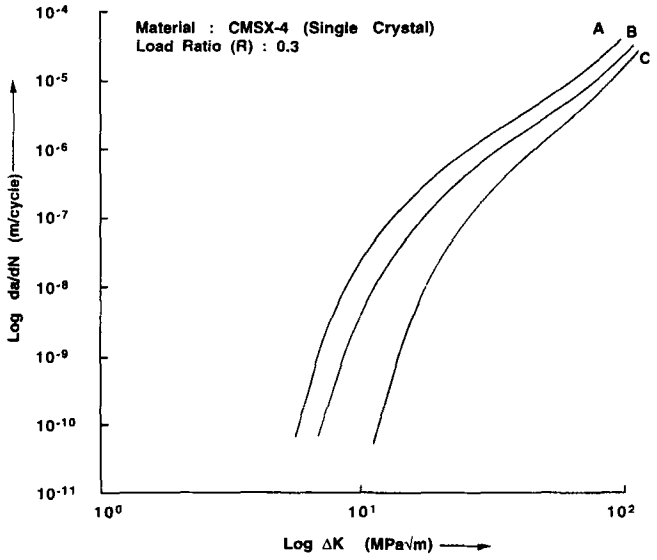

Fig. 4 Fatigue crack growth behavior at 650 °C

Table 2 Fatigue threshold of the material

Material condition	Load ratio, R	Fatigue threshold, MPa $m^{1/2}$
A	0.1	8.49
	0.3	5.92
	0.5	4.66
B	0.1	10.45
	0.3	7.09
	0.5	5.57
C	0.1	15.04
	0.3	11.74
	0.5	9.76

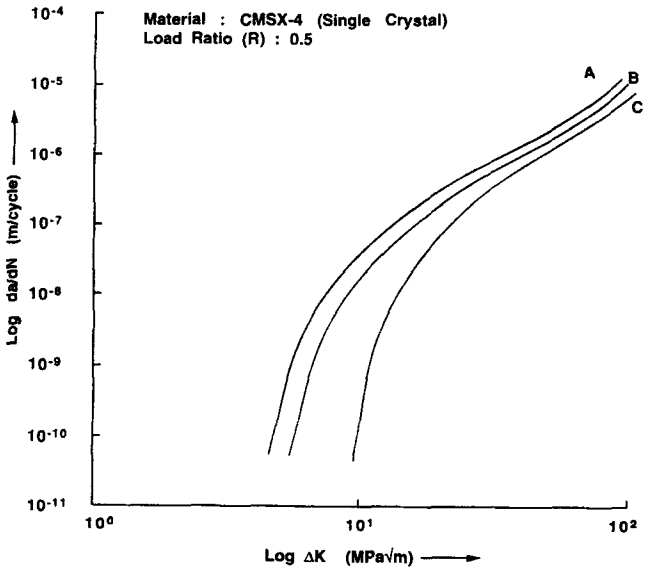

Fig. 5 Fatigue crack growth behavior at 650 °C

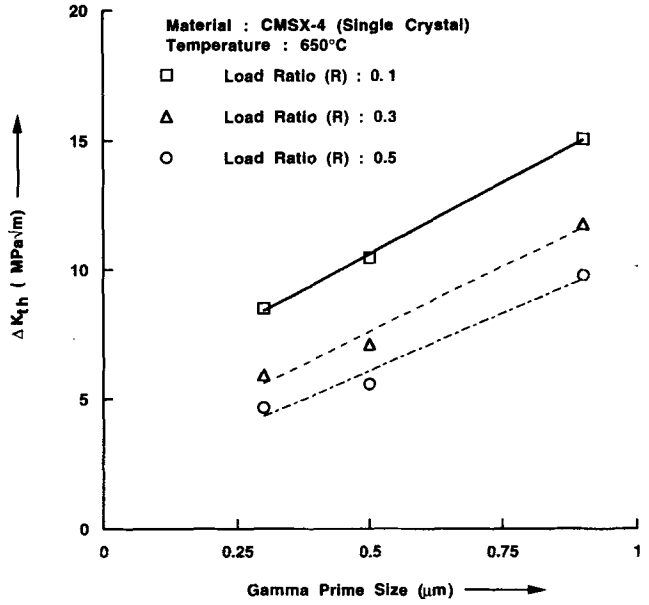

Fig. 6 Influence of γ' precipitate size on fatigue threshold, ΔK_{th}

However, this difference in crack growth rates decreases gradually as ΔK increases. In the very high ΔK region, the crack growth rates for A, B, and C specimens are very similar. Thus, the present test results indicate that as the γ' size increases, the near-threshold fatigue crack growth rate decreases at 650 °C. In Fig. 6, the fatigue threshold data of these materials are plotted against γ' precipitate size. This figure clearly shows that as γ' precipitate size increases the fatigue threshold value increases at 650 °C in CMSX-4. Hence, it is obvious that a larger γ' precipitate size is beneficial and will provide better fatigue crack growth resistance in the form of a higher fatigue threshold at 650 °C.

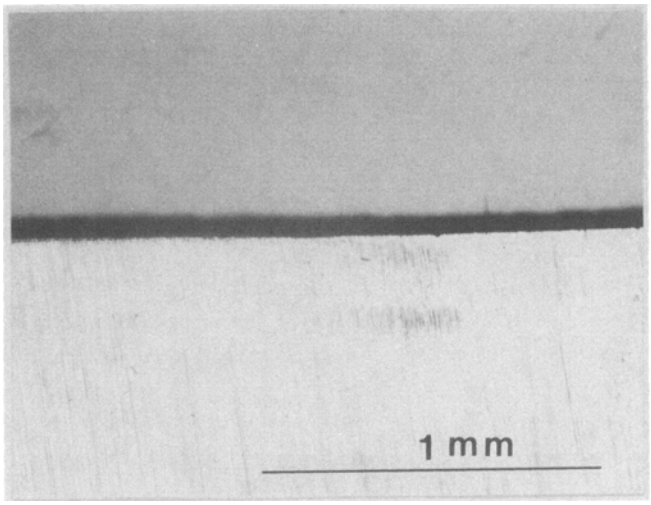

Fig. 7 Optical micrograph showing smooth fracture surface in the threshold region (heat treated condition A)

Figure 7 shows a macroscopic cross-section of the fracture surface along the thickness direction in the threshold region for heat treated condition A material. It shows a smooth fracture surface. Other specimens (Heat treated conditions B and C) also had similar smooth features on the fracture surface in the threshold region. Hence, these are not reported here. This relatively smooth and flat fracture surface (along the thickness direction) indicates stage II type of crack growth. This is indicative of a very homogeneous slip for all three heat treated conditions in the threshold region. This is also indicative of the predominantly stage II type of crack growth at the microscopic level.

Fractographs of these materials (A, B, and C) in the threshold region at 650 °C at load ratio R = 0.1 are shown in Fig. 8(a), (b), and (c), respectively. These figures indicate that the crack growth mechanism is basically the same (i.e., non-crystal-

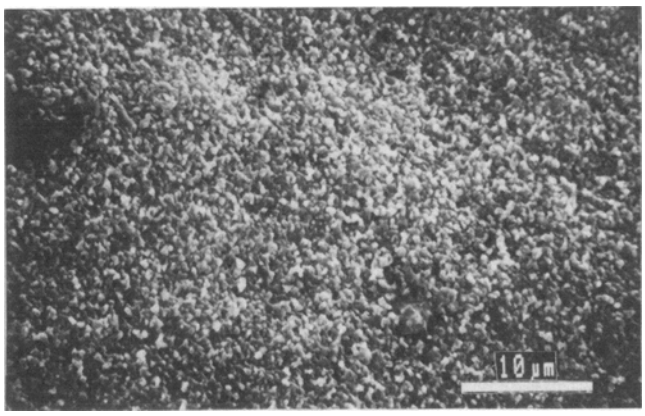

(a)

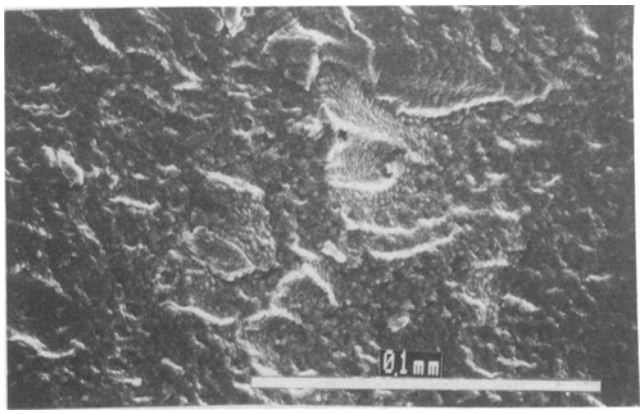

(b)

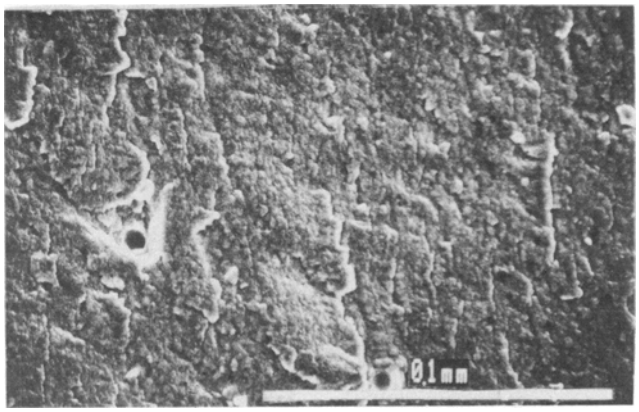

(c)

Fig. 8 Fractograph of heat treated condition A in the threshold region at 650 °C. (b) Fractograph of heat treated condition B in the threshold region at 650 °C. (c) Fractograph of heat treated condition C in the threshold region at 650 °C

lographic) in all these materials at 650 °C in the threshold region. Figure 9 is an optical micrograph of the fracture surface (along the thickness direction) in a high ΔK region for heat treated condition A material at load ratio R = 0.1. The optical micrograph of the other specimens (B and C) in the high ΔK region also had a similar appearance. The angular measurement of the angles between the crystal planes in Fig. 9 gave a value of 70.5°. This is one of the angular relationships, between {111} type of crystal planes.

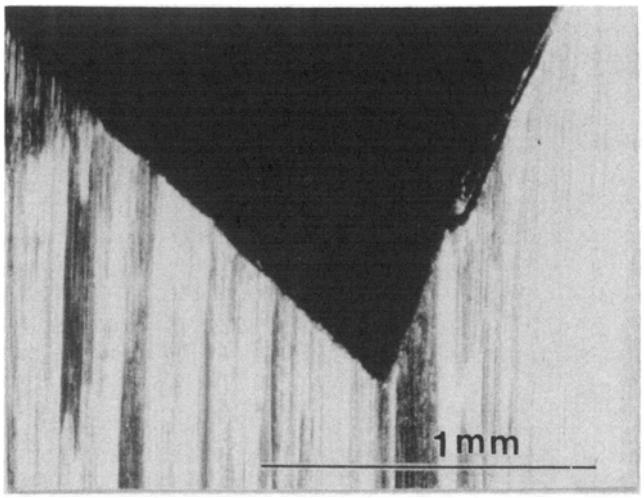

Fig. 9 Optical micrograph showing fracture along {111} planes in the high ΔK region (heat treated condition A)

The optical micrograph in Fig. 9 thus shows that the crack has propagated along {111} type of crystal planes in the high ΔK region. Fractographs at high ΔK region are shown in Fig. 10(a), (b), and (c). These also show a transition from stage II to stage I type of fracture in the very high ΔK regions, where cracks have been found to propagate in multiple {111} types of crystal planes. Some earlier work (Ref 14) has also reported similar phenomenon in PWA 1480 single crystal nickel-based superalloy.

This stage II type of crack growth in the threshold region, as observed in the present material, is related to the slip characteristics of the material. In single crystal nickel-based superalloys, high temperatures and low strain rates result in wavy, homogeneous slip (stage II), whereas low temperatures and/or high strain rates often produce planar heterogeneous slip (Ref 15) and crystallographic fatigue crack growth along {111} type of crystal planes (stage I). As the temperature increases, the transition from stage I to stage II crack growth occurs in the low ΔK region, and as a result smooth fracture surfaces are formed.

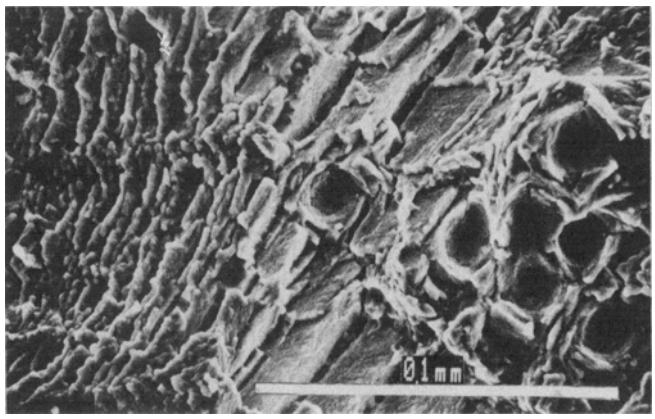

(a)

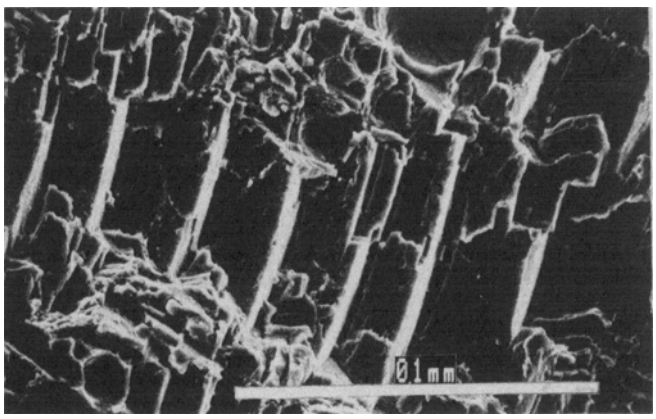

(b)

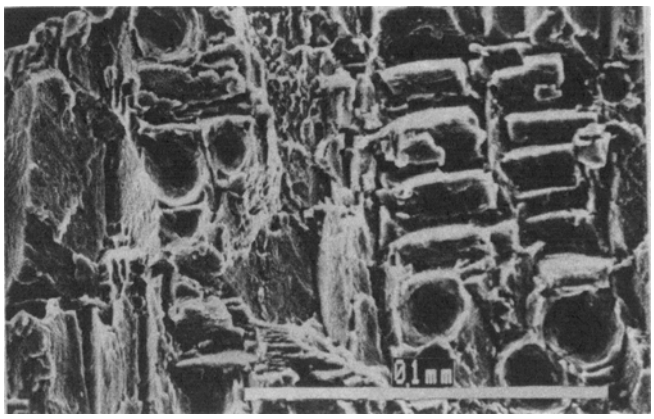

(c)

Fig. 10 (a) Fractograph of heat treated condition A in the fast fracture region at 650 °C. (b) Fractograph of heat treated condition B in the fast fracture region at 650 °C. (c) Fractograph of heat treated condition C in the fast fracture region at 650 °C

A thermally activated deformation process is involved, and planar slip bands of dislocations generate and are dispersed by thermally activated recovery processes such as dislocation climb or cross slip (Ref 15). The rate of this recovery process can be expressed by an Arrhenius-type relationship, i.e., rate~exp ($-\Delta H/RT$), where ΔH is the activation energy for the recovery process, R is the universal gas constant, and T is the temperature (in degree Kelvin). The value of this activation energy has been found to be comparable to the activation energy for creep processes in Ni-alloys (Ref 16, 17), as well as in single-phase γ, where diffusion-controlled climb was the rate controlling process.

At higher temperatures of 650 °C and lower ΔK (threshold region), this recovery process has led to stage II type of crack growth along {100} type of crystal planes in this material. With increasing ΔK, a large number of such bands can form on {111} type of slip planes (easy glide). At very high ΔK levels, higher crack growth rate limits the probability of dispersion of these dislocations, and this has led to stage I type of fracture in the intense slip bands along {111} type of planes as found in the present investigation. This also indicates that at very high temperatures, (T>800 °C), more thermal energy will become available for the dispersion of these dislocations and will result in homogeneous slip. This should again result in stage II type of fracture for the entire ΔK region. In fact, this has been found to be true in fatigue tests done at 800 °C on this material by the present investigators (Ref 18).

Since the fracture surface was relatively smooth at 650 °C in the threshold region, there was no significant roughness-induced crack closure (Ref 19) for all these specimens. Moreover, as reported in Table 3, the yield strengths of the heat treated conditions B and C materials were higher than for condition A material at this temperature. Hence, cyclic plasticity-induced crack closure (Ref 20) was lower for B and C materials compared to A material at 650 °C. Moreover, oxide-induced crack closure is expected to be similar for all these materials (A.

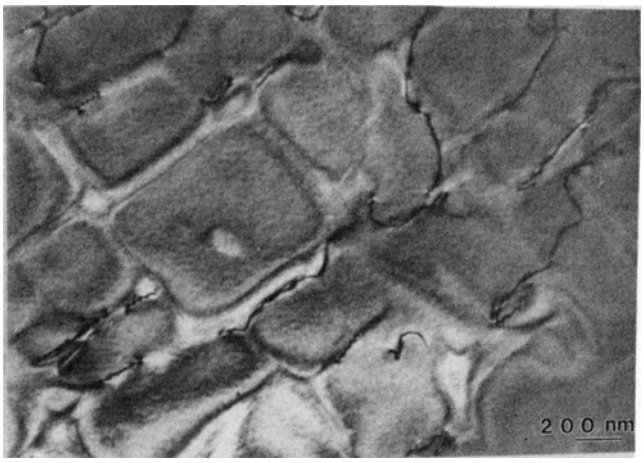

(a)

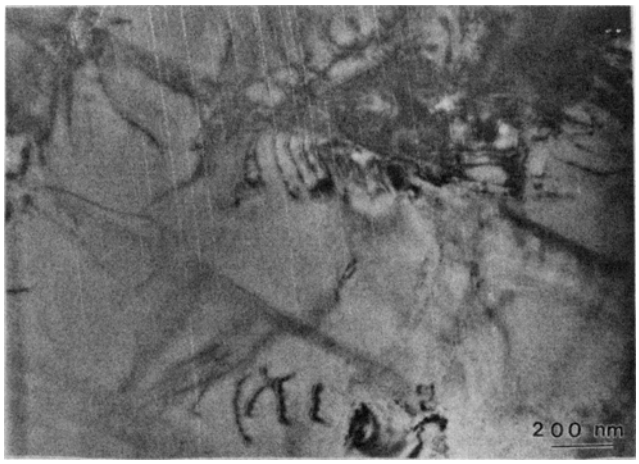

(b)

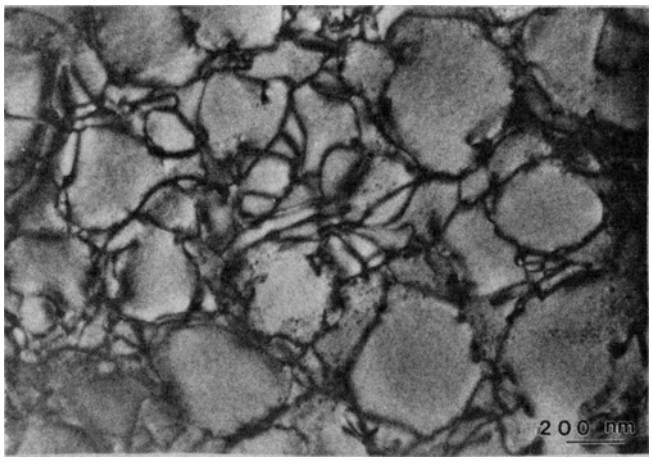

(c)

Fig. 11 (a) Transmission electron micrograph at 650 °C for heat treated condition A (in the threshold region). (b) Transmission electron micrograph at 650 °C for heat treated condition B (in the threshold region). (c) Transmission electron micrograph at 650 °C for heat treated condition C (in the threshold region)

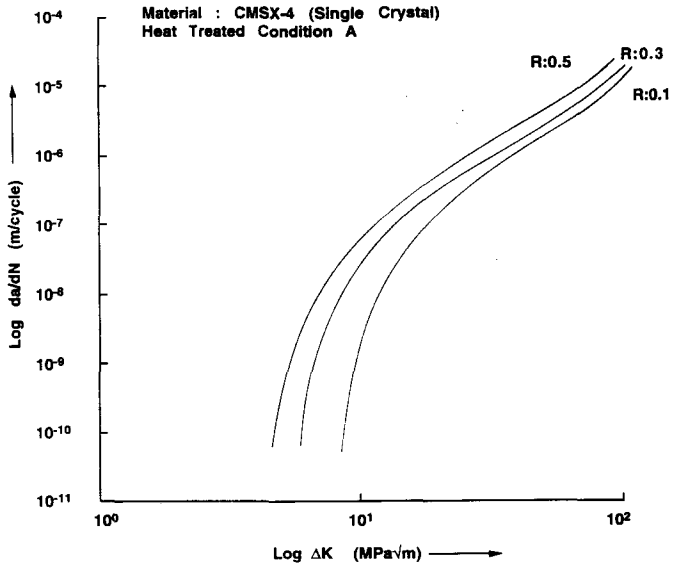

Fig. 12 Influence of load ratio on fatigue crack growth behavior at 650 °C

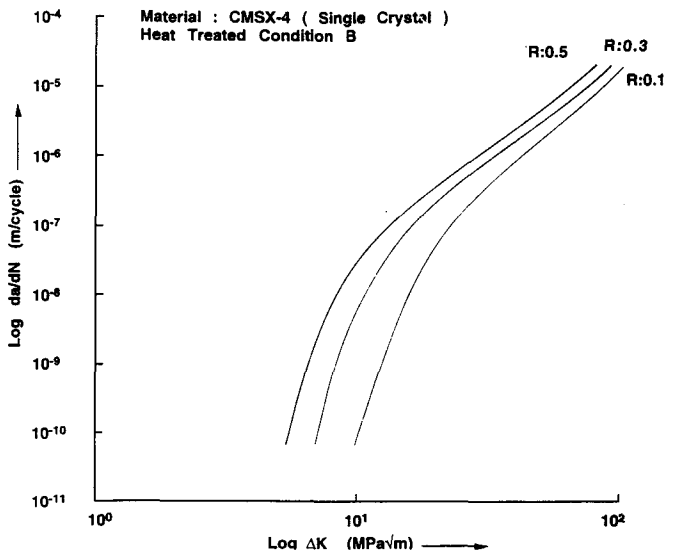

Fig. 13 Influence of load ratio on fatigue crack growth behavior at 650 °C

B, and C) at 650 °C. From this, one would expect a lower crack growth rate and higher fatigue threshold for heat treated condition A material than for B and C materials. However, as mentioned earlier, present test results show the opposite trend, i.e., the crack growth rate of material A was higher than B and C materials at this temperature. The reason for this behavior is discussed below.

Figures 11(a), (b), and (c) show transmission electron micrographs for A, B, and C materials. Heat treated condition A shows the presence of dislocations at the γ—γ' interface, whereas heat treated condition B (Fig. 11b) shows the presence of dislocation dipoles and superdislocations besides looping of dislocation around γ' precipitates. In addition, both of these figures show some cutting of the γ' precipitates by dislocations. On the other hand, the transmission electron micrograph of heat treated condition C material shows the breakdown of the γ' precipitates into smaller spherical shapes. In heat treated condition A, the presence of dislocations at γ—γ' phase boundaries indicates that climbing mechanisms are active (Ref 21-23). As the γ' precipitate size increases, the loop formations by dislocations around these γ' precipitate particles become increasingly more difficult (Ref 24). The presence of dislocation dipoles and superdislocations in heat treated condition B (Fig. 11b) confirms this (Ref 25, 26). Furthermore, as the γ' precipitate size increases, the shear stress necessary for shearing the γ' precipitates also increases (Ref 27). Presence of the interfacial dislocations [28] also indicate some dislocations more through the γ matrix by forced Orowan bowing, and this increases the resistance. The combined effect is increased resistance to dislocation motion as γ' size increases, and thereby increased fatigue crack growth resistance for heat treated condition B material compared to heat treated condition A material. Thus, the fatigue crack growth rate is lower and the fatigue threshold is higher for heat treated condition B material compared to heat treated condition A material at this temperature.

As mentioned earlier, the transmission electron micrograph for the heat treated condition C shows breakdown of cuboidal γ' and formation of smaller spherical γ' precipitates. It also shows the presence of homogeneous distribution of dislocations around precipitates (i.e., looping). Furthermore, some cutting of γ' precipitates by dislocations is also visible in this micrograph (Fig. 11c). During the thermomechanical process of high temperature fatigue, stress-induced diffusion can cause the breakdown (Ref 29) of γ' precipitates. In heat treated condition C, this breakdown has taken place. In this way the γ' precipitate structure has rearranged itself drastically in the form of coarsening of primary and formation of secondary precipitates during thermomechanical fatigue.

Due to this stress-induced breakdown, the γ' precipitates have taken predominantly spherical shapes. These spherical precipitates increase the resistance (Ref 29) of dislocation motion significantly. Furthermore, heat treated condition C had the highest yield strength, which is again indicative of high resistance to dislocation motions in this material. This increased resistance for dislocation motion in heat treated condition C will reduce its crack growth rate and has compensated the effect of lower crack closure due to its highest yield strength.

Thus, a combination of all these factors has resulted in the highest fatigue crack resistance at 650 °C for heat treated condition C material. The ultimate result is the lowest fatigue crack growth rate and highest fatigue threshold for heat treated condition C material compared to all other heat treated conditions. It is also interesting to note that this breakdown of cuboidal γ' into spherical γ' was not observed at 650 °C or at 800 °C (Ref 18) in either heat treated condition A or B material. Hence, it appears that there is a critical cuboidal size for γ' beyond which cuboidal γ' precipitates can break down due to stress-induced diffusion into smaller spherical particles. It appears such metastable γ' precipitate size will be highly desirable for maximum high temperature fatigue crack growth resistance and the fatigue threshold.

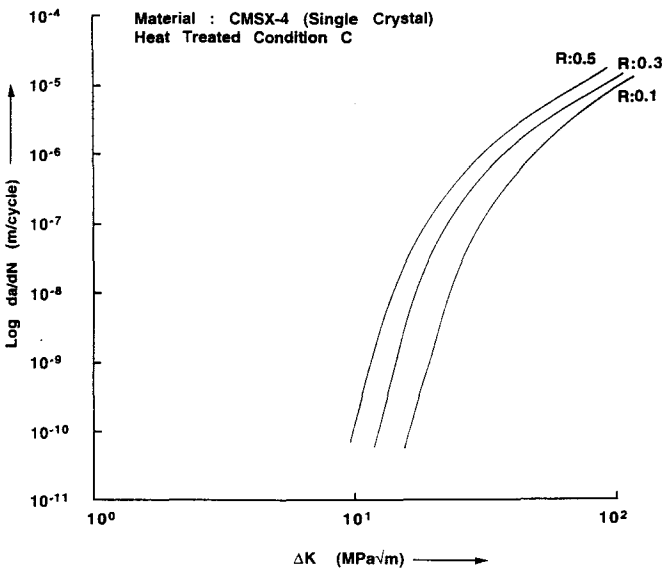

Fig. 14 Influence of load ratio on fatigue crack growth behavior at 650 °C

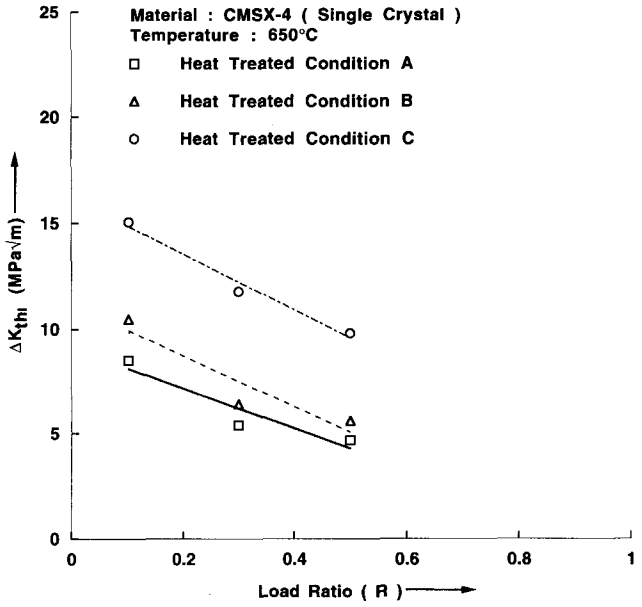

Fig. 15 Influence of load ratio on fatigue threshold

3.2 *Influence of Load Ratio on Fatigue Threshold and Crack Growth Rate*

Figures 12, 13, and 14 report the fatigue crack growth behavior for heat treated conditions A, B, and C materials at 650 °C at load ratios of R = 0.1, R = 0.3, and R = 0.5, respectively. These diagrams indicate that the load ratio has a significant influence on the near-threshold crack growth rate in CMSX-4 at 650 °C. The crack growth rate appears to increase with increases in the load ratio in threshold region at high temperature, unlike some other single crystal nickel-based superalloys (Ref 30, 31).

Generally, at high temperatures both creep and environmental interaction may occur, and as a result the mean stress or the load ratio has more influence on the crack growth rate than at room temperature (Ref 29, 30). At room temperature, a higher load ratio usually has the most influence on regions I and III of the Paris curve, and relatively little influence in the linear region. The load ratio usually increases the crack growth rate (da/dN) in the threshold region at room temperature as a result of the reduced crack closure effect, and enhances the early onset of region III crack growth.

The results reported in the above figures indicate that there is a considerable increase in crack growth rate with increases in load ratios at 650 °C for all these specimens. It has been suggested (Ref 32) that creep and environmental interactions can occur at higher temperature, and since the creep process is more dependent on maximum load, in a loading cycle, higher load ratios will increase the crack growth rate. The creep effect on this alloy at 650 °C is very small. This is due to the presence of rhenium in this alloy (Ref 33), which reduces the creep rate significantly. Therefore, it appears that the load ratio effect on the present material is due to the environmental interaction effect; i.e., a similar phenomenon like stress corrosion cracking superimposed on pure fatigue at this temperature increases (Ref 33) the overall crack growth rate.

Oxygen can diffuse into this alloy from the crack tip region (Ref 30). At 650 °C, this oxygen diffusion can occur along the dislocations, which in turn can pin these dislocations down and cause oxidation embrittlement. Since the embrittlement effect is strongly dependent on the maximum load, a higher load ratio increases the maximum load for a given stress intensity range and can increase the overall crack growth rate at 650 °C by increasing the embrittlement contribution. At room temperature, contributions due to oxidation embrittlement are negligible. Hence, such dramatic effects of load ratio were not observed in this material (Ref 11).

Figure 15 shows the influence of load ratio, R, on the fatigue threshold, ΔK_{th}, at 650 °C for heat treated conditions A, B, and C materials at 650 °C. This figure shows a linear relationship between the fatigue threshold and the load ratio.

Vosikovosky (Ref 34) analyzed the data from the literature concerning the effect of load ratio on the fatigue threshold, and found that in most cases the threshold decreases linearly with increases in load ratio. He proposed an empirical relationship of the nature $\Delta K_{th} = \Delta K_{th0}(1-bR)$, where ΔK_{th0} is the value of the threshold at load ratio R = 0, and b is a material constant. He also noted that both ΔK_{th0} and b increase with increases in the yield strength of the material. Barsom (Ref 35) has also observed a similar linear relationship between fatigue threshold and load ratio.

Knelsil and Lucas (Ref 36), on the other hand, observed a nonlinear power-law relationship between the threshold and the load ratio, and proposed a relationship of the nature $\Delta K_{th} = \Delta K_{th0}(1-R)^{\alpha}$ where α is a constant whose value depends on the environment. The present test results show that a linear relationship exists between the fatigue threshold and the load ratio in these materials, and therefore that Barsom or Vosikovosky's (Ref 34, 35) relationships are more appropriate for characterizing the influence of load ratio on the fatigue threshold in this material.

4. Conclusions

- The near-threshold fatigue crack growth rate in CMSX-4 has been found to decrease with increases in γ' precipitate size at 650 °C.
- Fatigue threshold values have been found to increase with increases in γ' precipitate size at 650 °C. This indicates that a larger γ' precipitate size is beneficial for fatigue crack growth resistance at elevated temperature.
- Fracture surfaces in the threshold region show stage II type of crack growth along {100} planes for all three heat treated conditions, whereas fracture occurs along {111} type of planes in the high ΔK region.
- For heat treated condition C, breakdown of the precipitates from cuboidal into spherical occurs due to stress-assisted diffusion. This results in the highest fatigue crack growth resistance in this alloy, reflected by the lowest fatigue crack growth rate in the threshold region and the highest fatigue threshold.
- There is a critical cuboidal size for γ' precipitates beyond which stress-induced diffusion can cause breakdown of the cuboidal precipitate. This metastable precipitate size will be ideal for fatigue crack growth resistance at elevated temperature.

Acknowledgments

The authors with to thank Dr. Ken Harris of Cannon-Muskegon Corporation, Muskegon, MI for financial support of this work. We are also grateful to Mr. Robert Plecki of Joliet Metallurgical Services, Joliet, IL, for technical support of this work.

References

1. P.C. Paris and F. Erdogan, A Critical Analysis of Crack Propagation Laws, *J. Basic Engg.*, Vol 85, 1963, p 528-534
2. "Standard Test Methods for Plane-Strain Fracture Toughness of Metallic Materials," ASTM E-399, *Annual Book of ASTM Standards*, Vol 03.01, 1992, p 506-536
3. S.D. Antolovich and J.E. Campbell, Fracture Properties of Superalloys, *Superalloy Source Book*, American Society of Metals, 1982, p 112-119
4. H.E. Collins and R.J. Quigg, Carbide and Intermetallic Stability in Advanced Nickel-base Superalloys, *Trans. ASM*, Vol 61 (No. 1), 1968, p 139-148
5. D.N. Duhl, Single Crystal Superalloys, Superalloys, Supercomposites, and Superceramics, Academic Press, 1989, p 149-182
6. P.R. Sahm and M.O. Spiedel, *High Temperature Materials in Gas Turbines*, Elsevier Scientific, 1974
7. K. Harris, G.L. Erickson, S.L. Sikkenga, W. Brentnall, J.M. Aurrecoechea, and K.G. Kubarych, Development of the Rhenium Containing Superalloys CMSX-4 & CM 186LC for Single Crystal Blade and Directionally Solidified Vane Applications in Advanced Turbine Engines, *Seventh Int. Symp. on Superalloys*, Sept 1992
8. K. Harris, G.L. Erickson, and R.E. Schwer, Process and Alloy Optimization for CMSX-4 Superalloy Single Crystal Airfoils, *Cost 501/505 Conf., High Temp. Matls. for Power Eng.*, (Liege, Belgium), 1990
9. J.S. Erickson, W.A. Owezarski, and P.M. Curran, Process Speeds Up Directional Solidification, *Metal Progress*, Vol 99, 1971, p 58-66
10. "Standard Test Methods for Measurement of Fatigue Crack Growth Rates," ASTM E-647, *Annual Book of ASTM Standards*, Vol 03.01, 1992, p 674-701
11. A. Sengupta and S.K. Putatunda, Kinetics of γ' Precipitation and Its Influence on Fatigue Crack Growth Behavior of a New Single Crystal Nickel-base Superalloy (CMSX-4) at Room Temperature, *J. of Matls. Eng. Performance*, Vol 2 (No. 1), 1993, p 57-68
12. A. Sengupta and S.K. Putatunda, Dynamic Strain Ageing in a New Single Crystal Nickel based Superalloy CMSX-4, *Journal of Testing and Evaluation* (in press)
13. A. Sengupta, S.K. Putatunda, L. Batosiewicz, J. Hangas, and P.J. Nailos, Tensile Behavior of a New Single Crystal Nickel Based Superalloy CMSX-4, *J. Matls. Eng. Performance*, Vol 3 (No. 1), 1994, p 73-82
14. J. Telesman and L.J. Ghosn, Accelerated Fatigue Crack Growth Behavior of PWA 1480 Single Crystal Alloy and Its Dependence on the Deformation Mode, *Superalloys 1988*, S. Reichman et al., Ed., TMS, 1988, p 615-624
15. G.R. Leverant and M. Gell, The Influence of Temperature and Cyclic Frequency on the Fatigue Fracture of Cube Oriented Nickel-base Superalloy Single Crystals, *Metall. Trans.*, Vol 6A, 1975, p 367-371
16. J.P. Dennison, R.J. Llewellyn, and B. Wilshire, *J. Inst. Metals*, Vol 95, 1967, p 115
17. P.A. Flinn, Theory of Deformation in Superlattices, *Trans. TMS-AIME*, Vol 218, 1960, p 145-154
18. S.K. Putatunda and A. Sengupta, Fatigue Crack Growth Behavior of a New Single Crystal Nickel-based Superalloy at 800 °C, *8th CIMTEC World Ceramic Congress, Forum on New Materials* (Faenza, Italy), July 1994
19. S. Suresh and R.O. Ritchie, A Geometric Model for Fatigue Crack Closure Introduced by Fracture Surface Roughness, *Metall. Trans.*, Vol 13A, 1982, p 1627-1631
20. W. Elber, "Damage Tolerance in Aircraft Structures," STP 486, ASTM, 1971, p 230-242
21. P.B. Hirsch et al., Electron Microscopy of Thin Crystals, Butterworths, 1967, p 180-189
22. U. Glatzel and M. Feller Kneipmeier, Microstructure and Dislocation Configuration in Fatigued [001] Specimens of the Nickel-based Superalloy CMSX-6, *Scripta Metall.*, Vol 25, 1991, p 1845-1850
23. W.W. Milligan and S.D. Antolovich, Yielding and Deformation Behavior of the Single Crystal Superalloy PWA 1480, *Metall. Trans.*, Vol 18A, 1987, p 85-95
24. P.H. Thorton, R.G. Davies, and T.L. Johnston, The Temperature Dependence of the Flow Stress of the γ' Phase based upon Ni_3Al, *Metall. Trans.*, Vol 1, 1970, p 207-218
25. G.R. Leverant and M. Gell, The Influence of Temperature and Cyclic Frequency on the Fatigue Fracture of Cube Oriented Nickel-base Superalloy Single Crystals, *Metall. Trans.*, Vol 6A, 1975, p 367-371
26. J.H. Zhang, Z.Q. Hu, Y.B. Xu, and Z.G. Wang, Dislocation Structure in a Single-Crystal Nickel-Base Superalloy during Low Cycle Fatigue, *Metall. Trans.*, Vol 23A, 1992, p 1253-1258
27. P. Beardmore, R.G. Davies, and T.L. Johnston, On the Temperature Dependence of Flow Stress of Nickel-based Alloys, *Trans. TMS-AIME*, Vol 245, 1969, p 1537-1545
28. T.M. Pollock and A.S. Argon, "Creep Resistance of CMSX-3 Nickel Base Superalloy Single Crystals, *Acta Metall.*, Vol 40, 1992, p 1-30
29. S. Kraft, R. Zanta, and H. Mughrabi, Aspects of High-Temperature Low-Cycle Thermo-Mechanical Fatigue of a Single Crystal Nickel-base Superalloy, *Fatigue and Fracture of Eng. Matls.*, Vol 16 (No. 2), 1993, p 236-253
30. M. Khobaib, T. Nicholas, and S.V. Ram, "Role of Environment in Elevated Temperature Crack Growth Behavior of René N4 Single

Crystal," STP 1049, W.B. Lisagor et al., Ed., ASTM, 1990, p 319-333

31. J.S. Crompton and J.W. Martin, Crack Growth in a Single Crystal Superalloy at Elevated Temperature, *Metall. Trans.*, Vol 15A, 1984, p 1711-1719

32. K.S. Chan, J.E. Hack, and G.R. Leverant, Fatigue Crack Growth in Mar-M200 Single Crystals, *Metall. Trans.*, Vol 18, 1987, p 581-591

33. A.F. Giamei and D.L. Anton, Rhenium Additions to a Ni-base Superalloy: Effects of Microstructure, *Metall. Trans.*, Vol 16A, 1985, p 1997-2005

34. O. Vosikovsky, Effect of Stress Ratio on Fatigue Crack Growth Rates in Steels, *Eng. Frac. Mech.*, Vol 11, 1979, p 595-602

35. J.W. Barsom, Fatigue Behavior of Pressure-Vessel Steels, *W.R.C. Bulletin*, Vol 194, 1974, p 33-45

36. M. Klensil and P. Lukas, Effect of Stress Cycle Asymmetry on Fatigue Crack Growth, *Mater. Sci. Eng.*, Vol 9, 1972, p 231-236